Models of orientational correlations in fluids: applications to liquid fluorine

1995 J. Phys.: Condens. Matter 7 483

(http://iopscience.iop.org/0953-8984/7/3/005)

J. Phys.: Condens. Matter 7 (1995) 483–497. Printed in the UK

Models of orientational correlations in fluids: applications to liquid fluorine

A De Santis†, A Gregson† and D Rocca‡

† Facolta' di Agraria, Universita' della Tuscia, Via S C De Lellis, 01100 Viterbo, Italy

‡ Dipartimento di Fisica, Universita' 'La Sapienza', Piazzale Aldo Moro 2, 00185 Roma, Italy

Received 8 July 1994, in final form 13 October 1994

Abstract. A new method of analysing the experimental atom–atom pair distribution functions $g_{aa}(r)$, based on the corresponding state principle, is presented. The method is first tested on nitrogen and chlorine liquids via computer simulations by exploiting intermolecular potentials that reproduce the experimental data satisfactorily. It is then applied to liquid fluorine to explain the large discrepancies we found when experimental and simulated $g_{aa}(r)$ were compared. Different models involving various degrees of microscopic orientational correlation are built up; among them, only one implying no appreciable orientational order agrees with the experimental data for fluorine. This model also fits liquid nitrogen well and fails in the case of liquid chlorine; consequently, the microscopic structure of liquid fluorine must be very different from that of other liquid halogens. However, some discrepancies between model and experimental $g_{aa}(r)$ of fluorine around 5 Å and spurious oscillations below 2 Å indicate that significant experimental uncertainties could affect the experimental data. The results of other models, which imply different degrees of orientational order, reported here can provide a useful guide for interpreting new experimental data.

1. Introduction

The structure factor $S(Q)$ and the related atom–atom radial distribution function $g_{aa}(r)$ obtained from neutron diffraction experiments have produced a significant contribution to the knowledge of liquid structure. The interest in diatomic liquids is due to the presence of orientational correlation between molecules, which influences diffraction measurements. To extract information about correlation is, however, a difficult task since all the quantities measurable by the neutron diffraction technique are averaged over the orientations of the molecules. So, recourse to a theoretical model or to computer simulations is necessary. In recent years, computer simulations exploiting sophisticated intermolecular potentials have produced significant improvements in the agreement between simulated and experimental pair correlation functions. Particular attention has been devoted to the liquid halogens, chlorine, bromine and iodine, for which anisotropic site potentials have been developed and several simulations [1, 2] and experimental works [3, 4] have been performed. In general, effective pair potentials fit the global shape of the atom–atom pair distribution function $g_{aa}(r)$: serious problems arise only when one needs to extract information about the microscopic structure.

Liquid F_2 is an exception. Indeed, for this liquid, only one experimental measurement [5] is available, only a two-centre Lennard-Jones potential model [6] has been proposed and no direct comparison between them exists. No effort has been made to build up a good potential for the liquid phase, other potential models having been developed for the solid

0953-8984/95/030483+15$19.50

Table 1. Triple (T_{tr}, V_{tr}) and reduced ($T^* = T/T_{tr}$, $V^* = V/V_{tr}$) values of temperature and molar volume for the various liquids. The values of the bond length l are those used in the potential models (section 2 of the main text); σ_{aa} and σ_e are the atomic site and mean 'excluded volume' diameters, respectively.

	T_{tr} (K)	V_{tr} ($m^3 \times 10^4$)	T^*	V^*	l (Å)	σ_{aa} (Å)	σ_e (Å)
Ar	83.8	0.282	1.44	1.22	—	—	3.405
N_2	66.6	0.321	1.44	1.15	1.098	3.20	3.55
F_2	53.5	0.222	1.44	1.10	1.427	2.70	3.14
Cl_2	172.2	0.407	1.45	1.13	1.994	3.20	3.85

phase [7] and in order to describe molecular dissociation and chemical reactivity in the fluid phase [8]. Furthermore, an attempt to extract information on the microscopic local order from the available experimental structure factor $S(Q)$ has failed [9].

We have devoted recent works to the study of the orientational order in diatomic liquids [10–13]. By developing the idea that the angular space of a pair $\Omega = (\omega_1, \omega_2)$ could be divided into a few disjoint classes of molecular orientations ω_1', ω_2', called microscopic configurations, it has been shown that it is possible to compare pair distribution functions of different liquids as well as to gain a reliable description of the microscopic structure. The method is particularly useful in analysing the experimental $g_{aa}(r)$ of liquid F_2, which is uncertain because of some experimental difficulties [14] discussed in detail in subsection 2.2, and appears to be in contrast with molecular dynamics (MD) simulation [6], at least initially for qualitative comparison. Since the direct comparison will show that the discrepancies are very strong, the main goal of the work is to recognize to what extent the experimental data are consistent with some models of diatomic liquids. For this purpose, the centre, $g_{cc}(r)$, and atom, $g_{aa}(r)$, distribution functions of liquid F_2 are derived from those of Cl_2, N_2 and Ar liquids by exploiting a new method of analysis. The paper is organized as follows: in section 2, experimental and simulation data are directly compared and the influence of the experimental uncertainties on the structure factor $S(Q)$ is critically discussed; in section 3, the way of comparing pair correlation functions of different liquids is illustrated. Liquids Ar, N_2, F_2 and Cl_2 in nearly the same corresponding state are considered and some models of $g_{aa}(r)$ for N_2 and Cl_2 are compared to MD results. These models are applied to liquid F_2 and a general discussion on the consistency between models and experimental data is reported in section 4; the summary of section 5 concludes the work.

2. Available experimental data and MD simulations

2.1. MD simulations

The MD technique has been used to simulate liquid Ar, N_2, Cl_2 and F_2. The potential models used have been the Lennard-Jones model for Ar with parameters taken from the second virial coefficient [15], the two-centre Lennard-Jones plus quadrupole model for N_2 [16], the anisotropic site model A2 for Cl_2 [1] and the two-centre Lennard-Jones model for F_2 [6]. The output configurations have been produced following the standard procedure described in [10]. All the liquids have been simulated by following the dynamics of 500 particles. The temperatures T and the molar volumes V of the thermodynamic states investigated are reported in table 1. The values correspond to thermodynamic points on the coexistence curve at the same reduced values $T^* = T/T_{tr}$, $V^* = V/V_{tr}$, T_{tr} and V_{tr} being the triple-point values.

2.2. *Experimental data and MD results for liquid F_2*

The only available diffraction measurement on liquid F_2 was performed at the thermodynamic state $T = 77$ K and $V = 0.2433 \times 10^{-4}$ m^3 [5]. The experimental structure factor $S(Q)$ and the related atom–atom pair distribution function $g_{aa}(r)$ are shown in figure 1(a) and (b), respectively. In [14], the quality of the experimental data has been judged insufficient to allow definitive conclusions about the presence of orientational correlation. The reasons are

(i) the use of a Monel alloy cell, imposed by the high degree of corrosivity of the liquid F_2, has produced sharp Bragg peaks in the 2.5–4.0 Å^{-1} range and caused some problems in subtracting the empty cell contribution and

(ii) the experiment was performed in a limited range of scattering angle so the maximum value of momentum transfer, Q, was about 8 Å^{-1}.

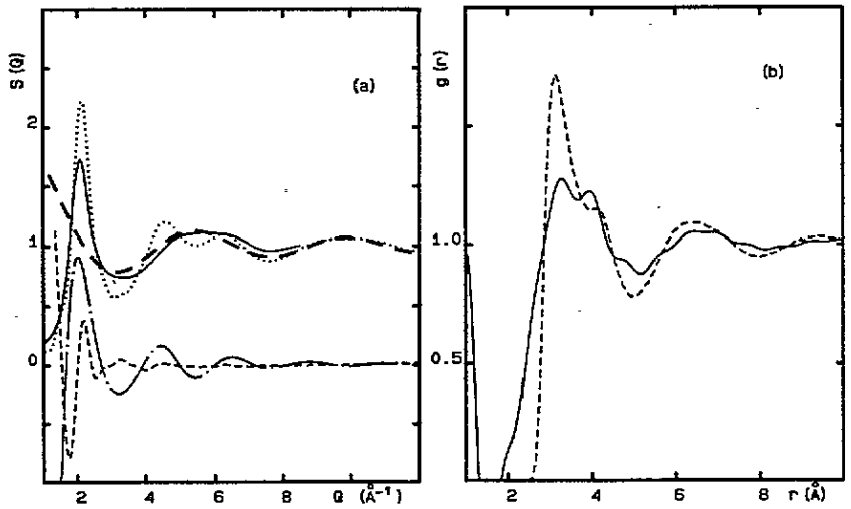

Figure 1. (a) Experimental (——) and simulated (· · · · · ·) total structure factors $S(Q)$, first-neighbour ($D_{aa}^{(f)}(Q)$, — · —) and next-neighbour ($D_{aa}^{(n)}(Q)$, (- - - -) structure factors and form factor $f_1(Q)$ (– – –) of liquid fluorine. (b) Experimental (——) and simulated (- - - -) atom–atom radial distribution functions of liquid F_2.

The uncertainty (ii) could seriously affect $g_{aa}(r)$ via truncation errors and invalidate any investigation of the orientational correlations performed in r space. It is therefore worth clarifying the Q range in which orientational correlations fall. This can be done by computer simulation, assuming that orientational correlations do not extend beyond the first coordination shell, i.e. beyond the first minimum of the centre–centre pair distribution function. This is valid in liquid Cl_2 [11] and the same rule can be reasonably extended to liquid F_2.

The experimental and simulated $S(Q)$ and $g_{aa}(r)$ are compared in figure 1(a) and (b), respectively. The discrepancies are very strong and mainly concern the atom–atom distribution of first-neighbouring molecules. The structure factor $S(Q)$ can be written as the sum of the first- (f) and next- (n) neighbour contributions and of the intramolecular form factor $f_1(Q)$, i.e.

$$S(Q) = f_1(Q) + D^{(n)}(Q) + D^{(f)}(Q) \tag{1}$$

where

$$f_1(Q) = \frac{1}{4}\sum_{\alpha,\beta}\left\langle \exp\left(iQ\cdot(r_{1\alpha}-r_{1\beta})\right)\right\rangle = \frac{1}{2}[1+\sin(Ql)/Ql] \tag{2}$$

$$D^{(f)}(Q) = 8\pi\rho\int_0^\infty dr r^2 g_{aa}^{(f)}(r)\sin(Qr)/Qr \tag{3}$$

$$D^{(n)}(Q) = 8\pi\rho\int_0^\infty dr r^2\left[g_{aa}^{(n)}(r)-1\right]\sin(Qr)/Qr. \tag{4}$$

Here α and β are indices of atomic sites in a molecule, $r_{1\alpha}$ and $r_{1\beta}$ are the centre–atom separation vectors, l is the bond length and ρ is the atomic density.

$g_{aa}^{(f)}(r)$ and $g_{aa}^{(n)}(r)$ have been obtained from molecules whose centres of mass fall in the first and next coordination shell, respectively. The functions $D^{(n)}(Q)$, $D^{(f)}(Q)$ and $f_1(Q)$ are shown in figure 1(a). As is seen, for $Q > 8$ Å^{-1} only $f_1(Q)$ gives significant contributions so the effects of the truncation on the orientational correlations in transforming the experimental $S(Q)$ can be neglected. In the region 4 Å^{-1} $< Q <$ 8 Å^{-1}, only $D^{(f)}(Q)$ and $f_1(Q)$ contribute, $D^{(f)}(Q)$ significantly modulating the $f_1(Q)$ signal. This indicates that the differences between simulation and experiment are not ascribable only to the experimental data corrections since the experimental spurious peaks, mentioned in (i), fall below 4 Å^{-1}. Therefore the MD simulation using the two-centre Lennard-Jones potential for liquid F_2 cannot be used to derive information on orientational correlations. To this end we will use a recently proposed method in the following [12].

3. Theoretical models

3.1. The complete set of orientation and the corresponding state principle

In this work the term configuration Γ is used to indicate a class of geometries of the isolated dimer. A configuration is chosen by progressively increasing the angular limits that define the geometry of a given oriented pair and verifying that the partial contribution to $g_{cc}(r)$ and $g_{aa}(r) * r^2$ does not change significantly in shape and in r position. Using this criterion, it has been shown [13] that the total configuration space $\Omega = (\omega_1, \omega_2)$ of linear molecules can be divided into at least five disjoint classes of configurations given by X($\theta_1 = 90° \pm 30°$, $\theta_2 = 90° \pm 40°$, $\phi = 90° \pm 30°$); T($\theta_1 = 90° \pm 40°$, $\theta_2 = 0° \pm 50°$, $0° < \phi \leqslant 360°$); LP($\theta_1 = 150 \pm 30°$, $\theta_2 = 30° \pm 30°$, $0° < \phi \leqslant 360°$); $\|$ ($\theta_1 = 75° \pm 15°$, $\theta_2 = 70° \pm 20°$, $-60° < \phi \leqslant 60°$), V($\theta_1 = 75° \pm 15°$, $\theta_2 = 110° \pm 20°$, $-60° < \phi \leqslant 60°$), where the polar and the azimuthal angles θ_1, θ_2 and $\phi = \phi_2 - \phi_1$ refer to the intermolecular vector. In this way we can write

$$g(r) = \sum_\Gamma g^\Gamma(r). \tag{5}$$

In figure 2 the total atom–atom and centre–centre radial distribution functions and the partial contributions $g^\Gamma(r)$ for N_2, F_2 and Cl_2 liquid are shown. As one can see, the differences between $g_{cc}(r)$ or $g_{aa}(r)$ of various liquids are due to differences in intensity and r position of the $g^\Gamma(r)$. To compare the $g_{cc}(r)$ of different liquids, it is therefore necessary to compare the $g^\Gamma(r)$ between them. Recently, a method based on the corresponding state principle has been proposed [12]. It exploits two scale constants, σ_e and σ^Γ, which represent the diameters

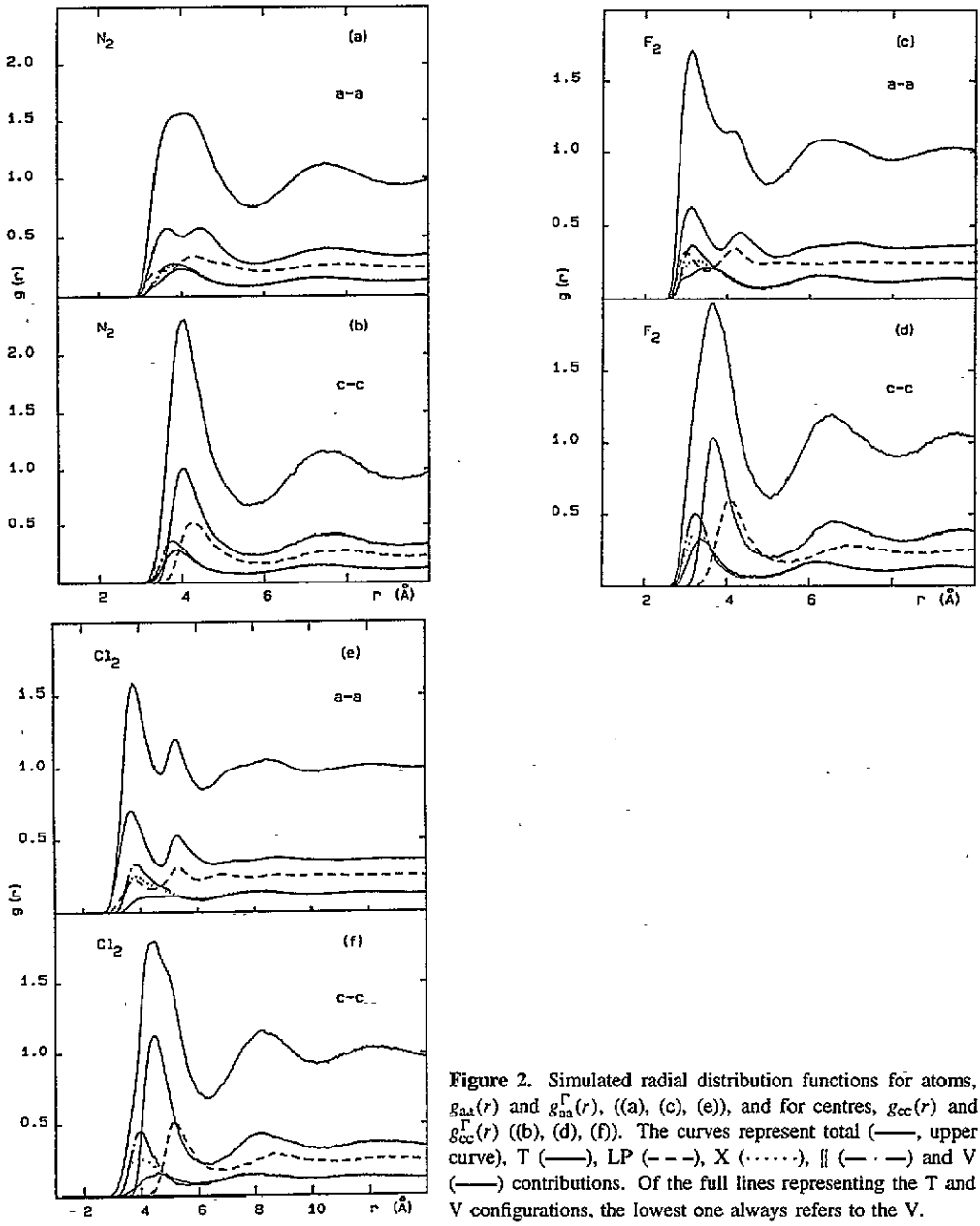

Figure 2. Simulated radial distribution functions for atoms, $g_{aa}(r)$ and $g^{\Gamma}_{aa}(r)$, ((a), (c), (e)), and for centres, $g_{cc}(r)$ and $g^{\Gamma}_{cc}(r)$ ((b), (d), (f)). The curves represent total (——, upper curve), T (——), LP (– – –), X (·····), ‖ (— · —) and V (——) contributions. Of the full lines representing the T and V configurations, the lowest one always refers to the V.

of the mean spherical volume excluded by a molecule and that of the mean volume excluded by a molecule involved in a configuration Γ, respectively. The distribution function

$$g_{cc}(r^*) = \sum_{\Gamma} \Omega^{\Gamma} G^{\Gamma}_{cc}(r^*) \tag{6}$$

where

$$G^{\Gamma}_{cc}(r^*) = \left(1/\Omega^{\Gamma}\right) g^{\Gamma}(r^*) \tag{7}$$

$$r^* = r/\sigma_e = (r - s^\Gamma)/\sigma_e \tag{8}$$

$$\Omega^\Gamma = \frac{1}{\Omega}\int\int_\Gamma\int d\theta_1\, d\theta_2\, d\phi \sin\theta_1 \sin\theta_2 \cos\phi \tag{9}$$

$$s^\Gamma = \sigma^\Gamma - \sigma_e \tag{10}$$

obeys a corresponding state principle: to a good approximation, it is a universal curve for liquids of linear molecules in corresponding state and reproduces the reduced distribution function of liquid Ar $g(r^*)$, where $r^* = r/\sigma_{Ar}$. The value of σ_e is obtained from

$$\sigma_e = \sigma_{Ar}\left(V_{tr}/V_{tr}^{Ar}\right)^{1/3} \tag{11}$$

where V_{tr} is the triple molar volume. In table 1, the values of σ_e are reported. The shifts s^Γ, and consequently σ^Γ, are determined by imposing that the parts of $G_{cc}^\Gamma(r)$ beyond the first coordination shell are as far as possible coincident. In figure 3 the functions $G_{cc}^\Gamma(r)$ of N_2, F_2 and Cl_2, obtained from the $g_{cc}^\Gamma(r)$ of figure 2(b), (d) and (f) respectively, via (7) and (10), are shown; the values of σ^Γ, determined by the applied shifts s^Γ, are reported in table 2. It is worth noting that σ^Γ can be easily estimated *a priori* without using MD data in the following way. A diatomic molecule is modelled by two fused hard spheres of diameter σ_{aa} whose centres are separated by the molecular bond length l (dumbbell model). The volume of this molecule is equivalent to that of a sphere whose diameter is given by [17]

$$\sigma_{hs} = \sigma_{aa}\left(1 + \tfrac{3}{2}l/\sigma_{aa} - \tfrac{1}{2}\left(l/\sigma_{aa}\right)^3\right). \tag{12}$$

By putting σ_{hs} equal to the mean spherical excluded volume σ_e, the atomic diameter σ_{aa} can be evaluated from (12). The results are reported in table 1. Then, from the dumbbell model, one calculates the mean centre distance of two molecules with two atoms in contact, as the polar angles vary in each configuration. The values σ_d^Γ obtained in this way are reported in table 2. As seen they are in good agreement with the values of σ^Γ.

Table 2. Values of the fraction of the solid angle Ω^Γ ((9) of the main text), of the average centre of mass distances of molecules in contact actually used, σ^Γ, and those computed from the dumbbell model, σ_d^Γ.

	X (Ω^Γ = 0.1309)		T (Ω^Γ = 0.3572)		LP (Ω^Γ = 0.2500)		‖ (Ω^Γ = 0.1309)		V Ω^Γ = 0.1309)	
	σ^Γ (Å)	σ_d^Γ (Å)	σ^Γ (Å)	σ_d^Γ (Å)	σ^Γ (Å)	σ_d^Γ (Å)	σ^Γ (Å)	σ_d^Γ (Å)	σ^Γ (Å)	σ_d^Γ (Å)
N_2	3.35	3.35	3.66	3.60	3.96	3.86	3.30	3.40	3.40	3.40
F_2	2.87	2.87	3.32	3.30	3.70	3.72	2.83	2.81	2.90	2.99
Cl_2	3.54	3.50	4.16	4.05	4.75	4.70	3.46	3.55	3.74	3.64

3.2. *The relation between centre–centre and atom–atom distribution functions*

For homonuclear diatomic liquids, the intermolecular structure factors of atoms and centres are given by

$$D_{aa}(Q) = \tfrac{1}{4}\left\langle \exp(iQ\cdot r_{12}) \sum_{\alpha,\beta} \left(iQ\cdot(r_{1\alpha} - r_{2\beta})\right)\right\rangle \tag{13}$$

$$D_{cc}(Q) = \left\langle \exp(iQ\cdot r_{12})\right\rangle \tag{14}$$

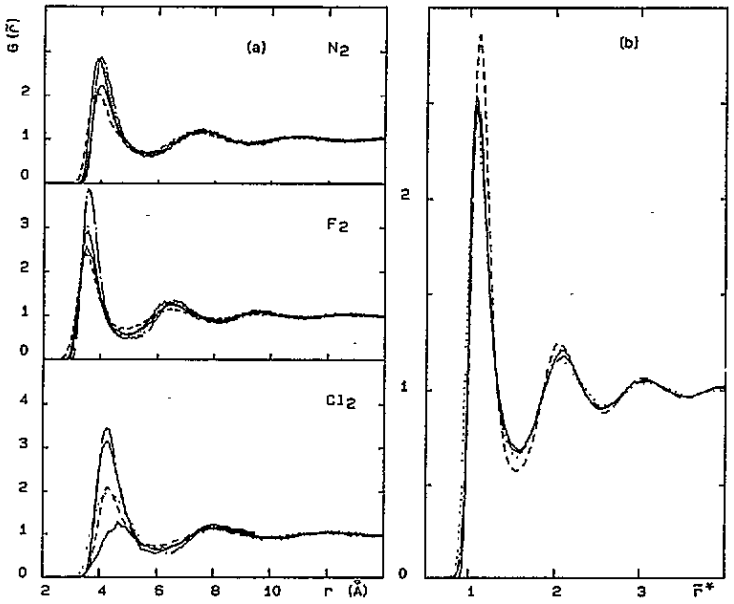

Figure 3. (a) Distribution functions $G^{\Gamma}_{aa}(r)$ obtained from the simulated $g^{\Gamma}_{cc}(r)$ of figure 2. For each fluid the curves represent T (——), LP (– – –), X (· · · · · ·) ‖ (— · —) and V (——). Of the two full lines, the lowest one represents the V configuration. (b) Distribution functions $g^{\Gamma}_{aa}(r^*)$ for Ar (——), N_2 (— · —), F_2 (– – –) and Cl_2 (· · · · · ·).

where $r_{\alpha\beta}$, r_{12} and $r_{1\alpha}$ are the atom–atom, centre–centre and centre–atom separation vectors respectively in a pair of molecules labelled 1 and 2.

The free rotation model (model I) [18] assumes the statistical independence of molecular positions and orientations. In this case one has

$$D_{aa}(Q) = f_{2u}(Q) * D_{cc}(Q) \tag{15}$$

where

$$f_{2u}(Q) = \frac{1}{4}\left\langle \sum_{\alpha,\beta} \exp(iQ \cdot r_{1\alpha}) \exp(iQ \cdot r_{2\beta}) \right\rangle = [\sin(Ql/2)/(Ql/2)]^2 \tag{16}$$

and the atom–atom radial distribution function can be obtained from

$$g_{aa}(r) = 1 + 8\pi\rho \int_0^\infty dQ\, Q^2 f_{2u}(Q) D_{cc}(Q) \sin(Qr)/Qr. \tag{17}$$

This model implies that the molecules are spherically distributed around a central one so that the centre structure factor $D_{cc}(Q)$ is that of a reference system whose properties are described by a spherically symmetric potential. For fluids of diatomic molecules the properties of liquid Ar in the corresponding state are usually exploited [14].

When the short-range repulsive forces are strongly anisotropic, the use of a spherical reference potential is expected to fail. (17) can be corrected along this line by choosing $D_{cc}(Q)$ of a non-spherical reference potential, by using, for example, MD results. An alternative route, which avoids the use of MD, is described in section 4. This way of correcting (17) will be denoted as the 'quasifree' rotation model or model II.

Further insight into the relation between centre–centre and atom–atom distribution functions can be obtained by introducing the configurations. Details of the centre–atom relationships obtained for the configurations in Q space and in r space are reported in [11] and [13], respectively. The results of interest here can be summarized as follows. By imposing the conservation of the number of interacting sites contained in a spherical shell of radius r and thickness dr, one obtains the following site–site distribution function in the intermolecular reference frame [13]:

$$\Delta g_{\alpha\beta}(r_{\alpha\beta}, \omega_1', \omega_2') r_{\alpha\beta}^2 dr_{\alpha\beta} = dr_{12} \int dr' \Delta g(r', \omega_1', \omega_2') r'^2 \delta(r' - r_{\alpha\beta} - d_{\alpha\beta}) \tag{18}$$

where $\Delta g(r, \omega_1, \omega_2)$ is the contribution of the orientations $\omega_1 \pm \Delta\omega$, $\omega_2 \pm \Delta\omega$ to the angular radial distribution function, δ is the Dirac delta function, and the parameter $d_{\alpha\beta}(r, \omega_1', \omega_2')$ can be calculated from the dimer geometry as

$$d_{\alpha\beta}(r, \omega_1', \omega_2') = r_2 - r_{\alpha\beta} = |r_{12}| - |r_{12} - r_{1\alpha} + r_{2\beta}|. \tag{19}$$

The total $\Delta g_{aa}(r, \omega_1', \omega_2')$ obtained from (18) is given by

$$\Delta g_{aa}(r, \omega_2', \omega_2') = \frac{1}{4} \sum_{\alpha\beta} \frac{dr_{12}}{r_{\alpha\beta}^2 dr_{\alpha\beta}} \int dr' g(r', \omega_1', \omega_2') r'^2 \delta(r' - r_{\alpha\beta} - d_{\alpha\beta}). \tag{20}$$

By averaging over a configuration Γ one has

$$g_{aa}^{\Gamma}(r) = \frac{1}{4} \sum_{\alpha\beta} \frac{dr_{12}}{r_{\alpha\beta}^2 dr_{\alpha\beta}} g_{cc}^{\Gamma}(r_{\alpha\beta}) (r_{\alpha\beta} + d_{\alpha\beta}^{\Gamma})^2 \tag{21}$$

where $g^{\Gamma}(r) = \langle g(r, \omega_1', \omega_2') \rangle_{\Gamma}$ and $g_c^{\Gamma}(r_{\alpha\beta})$ is the centre–centre distribution function shifted from the position r_{12} to the position $r_{\alpha\beta} = r_{12} + d_{\alpha\beta}$. (21) gives very good results for a small set of geometries centred around the orientations ω_1', ω_2' [13]. When the angular limits of a configuration Γ grow, some assumptions are necessary since several site–site distances $r_{\alpha\beta}$ could correspond to a given centre–centre distance r_{12}. Here two approximations are considered.

(i) For a given r_{12}, $r_{\alpha\beta}$ can assume all the possible values as the polar angular vary in the configuration. The intensity of $g_{cc}(r_{12})$ is then distributed over the range spanned by $r_{\alpha\beta}$ with a law derivable from a freely rotating dumbbell. Details of this method are reported in the appendix. This model, referred to as model III, is similar to a 'quasifree' rotation model (model II) in which the reference potential is not spherically symmetric, being determined by the molecular shape. Short-range repulsive anisotropic forces determine different r positions of each $g_{cc}^{\Gamma}(r)$ but no preferred orientation exists in a given configuration Γ. With respect to model II, however, a significant improvement has been obtained since specific operations are used to obtain each $g_{aa}^{\Gamma}(r)$ from each $g_{cc}^{\Gamma}(r)$. By contrast, (15) implies, in the r space, a convolution with the same function for every $g_{cc}^{\Gamma}(r)$.

(ii) The correspondence r_{12}, $r_{\alpha\beta}$ is one to one and, for every r_{12}, $r_{\alpha\beta}$ and $d_{\alpha\beta}$ are chosen as the mean values they assume as the polar angles vary in the configuration. Simple ways of computing such mean values are reported in the appendix. This model, hereafter referred to as model IV, implies the presence of preferred orientations, so one can expect that it holds for highly correlated fluids.

4. Results and discussion

Our purpose is to understand whether the experimental data agree with one of the models of $g_{aa}(r)$ described in section 3. Since N_2 and Cl_2 give rise, respectively, to weakly and strongly correlated liquids whose experimental $g_{aa}(r)$ are well reproduced by MD simulations, it is worth first applying the models to these liquids. In this way one can establish the model capability of representing more or less correlated liquids.

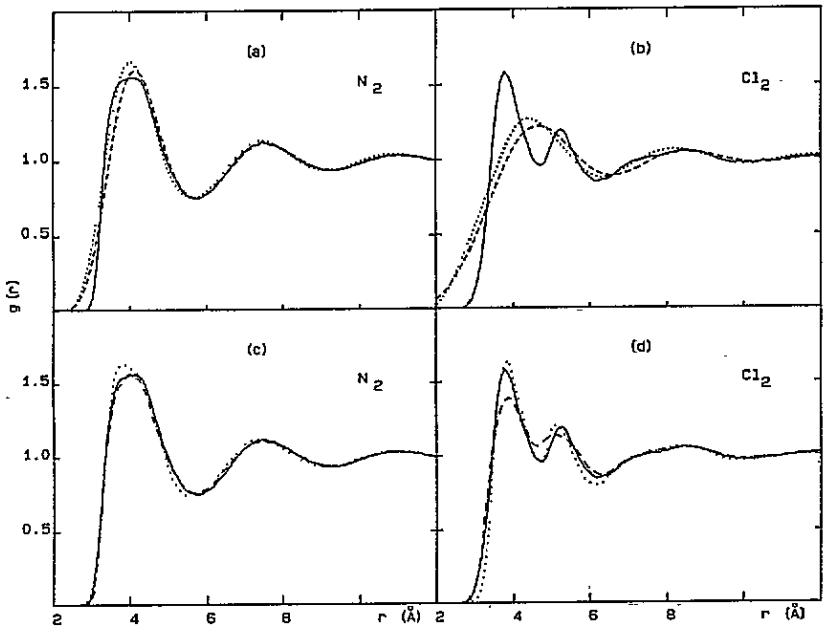

Figure 4. A comparison between simulated (——) and model $g_{aa}(r)$. In (a) and (b) the results of model I (·····) and model II (– – –) are shown; in (c) and (d) those of models III (– – –) and IV (·····) are shown.

The results of applying models I and II are shown in figure 4(a) and (b) for N_2 and Cl_2, respectively. Both the models fail completely in the case of Cl_2 while they work fairly well for N_2. The correction obtained by putting the real $g_{cc}(r)$ (model II) in place of the Ar-like one has a very small effect. The disagreement between the model and real $g_{aa}(r)$ of Cl_2 is due to the double-peak structure, which is not reproduced at all by the models. The factor $f_{2u}(Q)$ in (17) cancels the different r positions of each $g^{\Gamma}_{cc}(r)$ visible in figure 2(b), (d) and (f). When a specific operator is applied to each $g^{\Gamma}_{cc}(r)$ (models III and IV) the agreement is greatly improved, as figure 4(c) and (d) show. For N_2 and Cl_2, the properties of the non-spherical reference potential are simulated by dumbbells with hard atomic cores of 3.20 Å and 3.25 Å, respectively. Such values correspond to the r positions in which the real $g_{aa}(r)$ start to be significantly different from zero. As is seen, model III gives a very good description in the case of N_2 but fails for Cl_2. By contrast, model IV is fair for Cl_2 but shows some discrepancies in reproducing the shape of the first $g_{aa}(r)$ peak of N_2. In conclusion, models III and IV are particularly suitable for describing weakly and strongly correlated systems, respectively.

It is now possible to investigate the presence of orientational correlations in liquid F_2. For this purpose, the application of the models III and IV is sufficient. We will proceed as follows. (i) Centre–centre distribution functions are built up from the corresponding state principle. In this way, the differences in populations of configurations predicted by different anisotropic reference potentials are considered. (ii) The models III and IV are applied to each $g_{cc}(r)$ obtained in this way.

From (6), one obtains

$$g_{cc}(r) = \sum_{\Gamma} \Omega^{\Gamma} G^{\Gamma}_{cc}\left[\left(r^*\sigma_e\right) + s^{\Gamma}\right] \tag{22}$$

where σ_e and s^{Γ} are those of F_2 while $G^{\Gamma}_{cc}(r^*)$ are taken from the reference fluid. The values of σ_e and σ_d^{Γ} for liquid F_2 are reported in tables 1 and 2. The liquids of Ar, N_2 and Cl_2 are used as reference liquids and the different populations of each configuration are accounted for by the $G^{\Gamma}_{cc}(r^*)$. For liquid Ar, the functions $G^{\Gamma}cc(r^*)$ coincide with $g_{cc}(r^*)$, where $r^* = r/\sigma_{Ar}$. The three $g_{cc}(r)$ resulting from (22) are shown in figure 5. As is seen, the main differences are in the first-peak height, the uniform distribution of Ar giving the broadest and lowest first peak.

The three atom–atom distribution functions obtained from each $g_{cc}(r)$ are compared with the experimental data in figure 6(a) in the case of model III and in figure 6(b) in the case of model IV. In applying model III the atomic hard cores have been chosen equal to 2.0 Å as suggested by the experimental $g_{aa}(r)$. As is seen, all the $g_{aa}(r)$ reproduce the right r positions of the two peaks at 3.2 and 4.0 Å. Model IV (figure 6(b)) yields a $g_{aa}(r)$ sharper than the experimental ones independent of the reference liquid we use for deriving the centre distribution functions. This means that the different populations of the configurations can explain small rearrangements in height of the two peaks but cannot give the broadening required by the experimental data. The predictions of model III (figure 6(a)) are in quite good agreement with the experiments; the best agreement arises from the centre–centre distribution function predicted by liquid Ar, that is, by a uniform distribution of the intensity of the configurations. In conclusion, the available experimental data on liquid F_2 are consistent with a model in which no preferred orientation exists. This fluid appears more similar to liquid N_2 than to the other liquid halogens. This similarity is also confirmed by the solid phase: both crystalline N_2 and F_2 transform to a plastic cubic phase (β phase) before melting in which molecules are nearly freely rotating [7]. On the other hand, some details of the experimental data suggest caution before drawing definitive conclusions. There are oscillations of the experimental $g_{aa}(r)$ before 2.0 Å, which are probably due to noise. Their influence on the double structure of the first peak could be relevant. Indeed, around the first minimum at 5.0 Å, the experimental $g_{aa}(r)$ show a small bump followed by successive oscillations. If the behaviour of each partial contribution $g^{\Gamma}_{aa}(r)$ is considered (figure 7), one can see that the third smoothed peak of the LP configurations falls effectively around 5.0 Å, but there are no other structures capable of explaining the oscillations of the experimental data. Therefore, a noise signal probably affects the experimental data over all the r range and makes the conclusions suggested here uncertain. Moreover, the potentials developed for the solid phase [7] and those describing molecular dissociation in fluid [8] give a $g_{aa}(r)$ more similar to the MD results of [6] than to the experimental data. The differences between the predictions of the models investigated here are not limited to small details, as in the case of N_2 (figure 4(a) and (c)), but involve large differences in broadening and rising of the first two peaks (figure 6(a) and (b)); a new experimental measurement could definitively clarify the degree of microscopic orientational order present in liquid F_2.

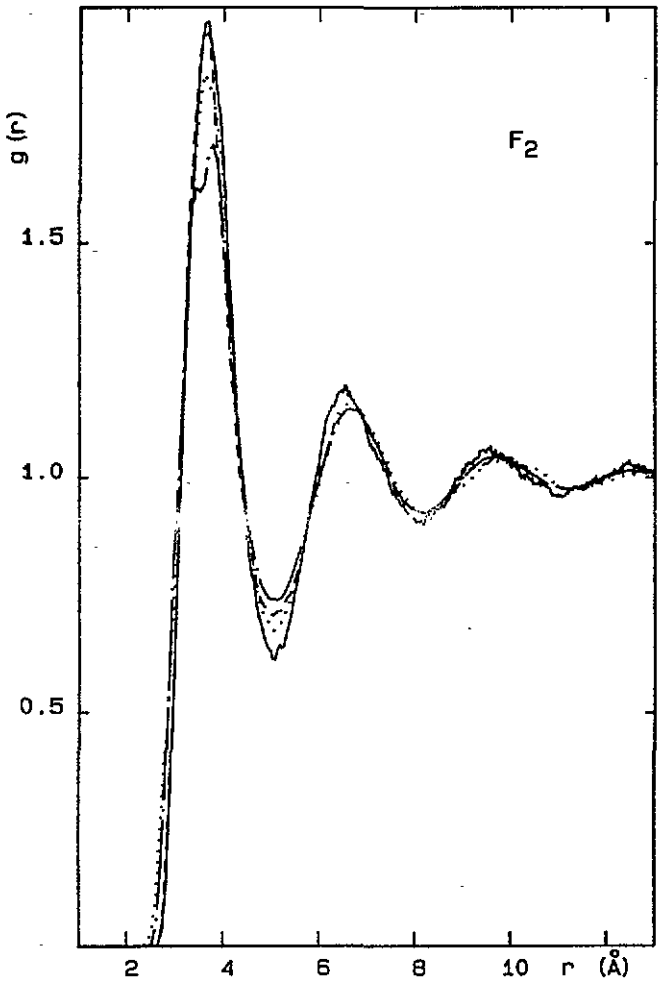

Figure 5. $g_{cc}(r)$ of F_2 obtained from MD (——) and from Ar (— · —), N_2 (– – –) and Cl_2 (· · · · · ·) via (22) of the main text.

5. Summary

The method of analysis applied here is based on the existence of a universal curve representing the $g_{cc}(r)$ of liquids in corresponding state. Such a curve is well reproduced by the $g(r^*)$ of liquid Ar, which can therefore be exploited as a reference liquid where no orientational correlation is present. To compare or derive the $g_{cc}(r)$ of different liquids one needs to know two basic parameters, the mean spherical excluded volume diameter σ_e and the bond length l. Both are derivable from literature, σ_e only requiring the application of the corresponding state principle (11). Further, it is shown that only a finite and small number of disjoint classes of orientations determines the main features of the pair distribution functions; it is then possible to derive the diameters σ^Γ of the volume excluded by a molecule for each configuration Γ. This yields a reliable estimate of the shifts s^Γ, which are the main effect produced by the anisotropic potential. The other effects concern the shape and population of the $g_{cc}^\Gamma(r)$, which are due to the details of the intermolecular potentials, such as the competition between non-spherical shape forces and electrostatic

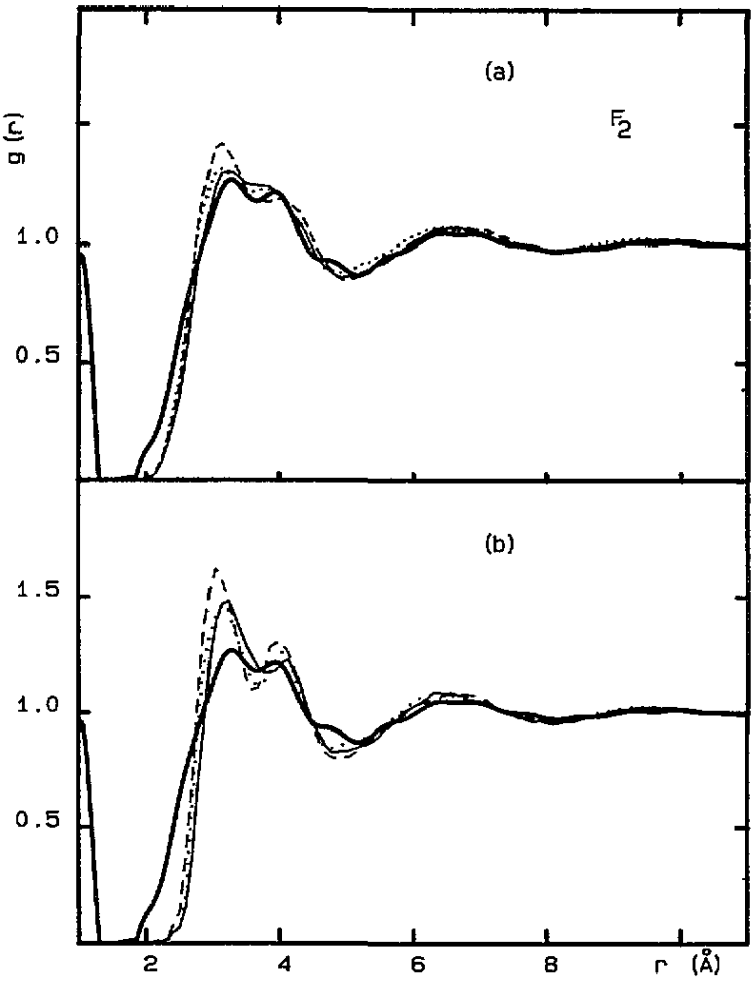

Figure 6. A comparison between experimental (——) and model $g_{aa}(r)$ of liquid F_2: (a) results of model III obtained from Ar (·····), N_2 (——) and Cl_2 (– – –) via (22) of the main text; (b) as in (a) but for model IV.

quadrupolar forces discussed in [18]. Therefore, no exact *a priori* prediction is possible. However, we can estimate the trend of the centre distribution function when each $g_{cc}^{\Gamma}(r)$ evolves from the uniform distribution of Ar to that of orientationally correlated liquids. In the case of liquid F_2, the better knowledge of the N_2 and Cl_2 liquids has been exploited. N_2 is a slightly anisotropic molecule where the 'free rotation' approximation works well and a simple 2LJQ potential is sufficient for modelling the real liquid [16]. By contrast in Cl_2 the short-range forces are strongly anisotropic and a more sophisticated pair potential with anisotropic interacting sites is required [1]. Figure 5 shows how the differences between the populations of $g_{cc}^{\Gamma}(r)$ can affect the total $g_{cc}(r)$ of liquid F_2. As is seen, the bond length of F_2 is not sufficient to evidence separate contributions of each $g_{cc}^{\Gamma}(r)$.

The same comparison can be performed between $g_{aa}(r)$ where the contributions of the different configurations are better separated in their r positions and the experimental information is accessible. Two possible ways of deriving atom–atom from centre–centre distribution functions, which work well in the case of N_2 and Cl_2 liquids, are exploited

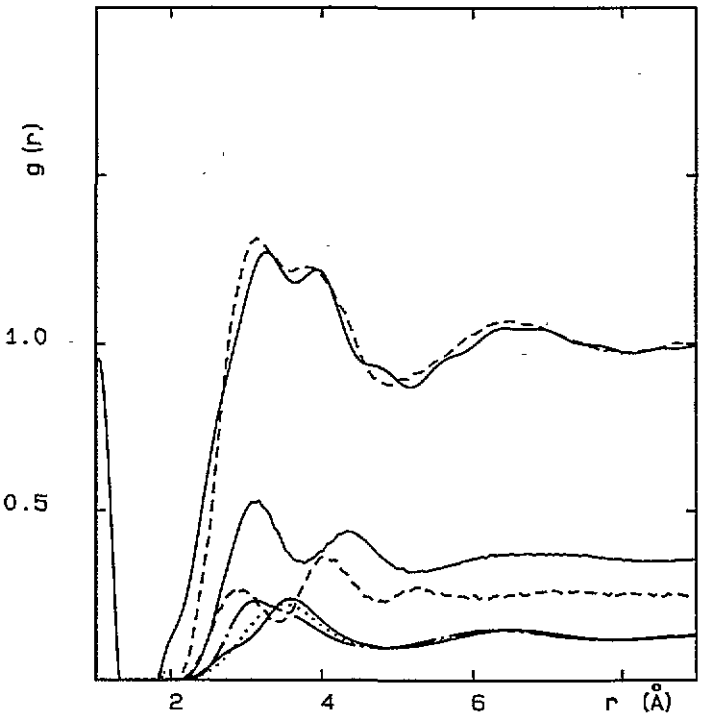

Figure 7. A comparison between $g_{aa}(r)$ of liquid F_2: experimental (——) (top) and from model III (– – –) obtained using Ar data. The partial $g^{\Gamma}_{aa}(r)$ obtained from model III are also reported: T (——), LP (– – –), X (·····), ‖ (— · —) and V (——) contributions. Of the lower two full lines, the lowest one represents the V configuration.

and the results are shown in figure 6(a) and (b). The differences between the model predictions are significant. The available experimental data are consistent only with a 'quasifree' rotation model. The differences in populations between configurations play a minor role, the less correlated cases of N_2 and Ar giving, however, the better results. So, the liquid F_2 appears to be more similar in its microscopic structure to the N_2 liquid than to the other liquid halogens. This conclusion should be however confirmed by other experimental data, since those available are probably affected by noise signals.

Appendix

The vector distance between the sites α and β, belonging to molecules 1 and 2 respectively, is given by

$$r_{\alpha\beta} = r_{12} - r_{1\alpha} + r_{2\beta} \tag{A1}$$

where $r_{1\alpha}$ and $r_{2\beta}$ are vectors pointing from the centre to the site and r_{12} is the centre of mass distance. If the z axis of the reference system coincides with the polar axis, the components of $r_{\alpha\beta}$ are

$$\begin{aligned} x_{\alpha\beta} &= -(l/2)(-\sin\theta_1\cos\phi_1 + \sin\theta_2\cos\phi_2) \\ y_{\alpha\beta} &= (l/2)(-\sin\theta_1\sin\phi_1 + \sin\theta_2\sin\phi_2) \\ z_{\alpha\beta} &= (l/2)(-\cos\theta_1 + \cos\theta_2) + r_{12} \end{aligned} \tag{A2}$$

where the polar angles θ and ϕ specify the molecular orientation ω and l is the bond length. To obtain the shift $d^{\Gamma}_{\alpha\beta}$, one needs to average $r_{\alpha\beta}$, since the components (A2) are not independent variables. A simple analytical solution can be obtained using the approximation $\langle |r_{\alpha\beta}| \rangle \simeq \sqrt{\langle r^2_{\alpha\beta} \rangle}$. One has

$$d^{\Gamma}_{\alpha\beta} \simeq \sqrt{\langle r^2_{\alpha\beta} \rangle} - r_{12} \tag{A3}$$

and by putting $\phi = \phi_2 - \phi_1$ equations (A2) yield

$$r^2_{\alpha\beta} = \frac{l^2}{4}\left(\sin^2\theta_1 \cos^2\phi_1 + \sin^2\theta_2 \cos^2\phi_2 - 2\sin\theta_1 \sin\theta_2 \cos\phi\right) + \frac{l^2}{4}\left(\cos^2\theta_1 + \cos^2\theta_2\right) - l r_{12}\left(-\cos\theta_1 + \cos\theta_2\right) + r^2_{12} \tag{A4}$$

so that the average

$$\langle r^2_{\alpha\beta} \rangle_{\Gamma} = \left(\int\int_{\Gamma}\int r^2_{\alpha\beta} \sin\theta_1 \sin\theta_2 \, d\theta_1 \, d\theta_2 \, d\phi\right) \Big/ \left(\int\int_{\Gamma}\int \sin\theta_1 \sin\theta_2 \, d\theta_1 \, d\theta_2 \, d\phi\right) \tag{A5}$$

becomes analytically solvable from elementary integration formulas [19].

Alternatively, equation (A4) can also be used to compute the mean value of $r_{\alpha\beta}$ for fixed centre distances r_{12} as the polar angles run over the configuration Γ. The mean values have been obtained by weighting every $r_{\alpha\beta}$ with the relative frequency of its occurrence $f_{\alpha\beta}$. Both methods lead to fair agreement between model and MD $g^{\Gamma}_{\alpha\beta}(r)$ for angular limits of $\pm 5°$.

When the angular limits grow, for every value of r_{12} one should take proper account of the spread of values assumed by $r_{\alpha\beta}$ as the polar angles run over the selected configuration Γ. In model IV this effect is neglected, thus obtaining model distribution functions slightly sharper than the MD ones (figure 4(c), (d)). In model IV, the frequency distribution $f_{\alpha\beta}$ has been used to compute the spread in $r_{\alpha\beta}$ by assuming that no preferred orientation exists as the polar angles run over a given configuration Γ. Equality between the number of centres contained in the elementary spherical volume of radius r and thickness dr and the number of sites distributed over the interval r_a, r_b is obtained from

$$dN^{\Gamma} = g^{\Gamma}_{cc}(r) r^2 \, dr = dA \int_{r_a}^{r_b} dr r^2 f^{\Gamma}_{\alpha\beta}(r) \tag{A6}$$

where dA is a normalization factor. The elementary site–site distribution function is

$$dg^{\Gamma}_{\alpha\beta}(r) = f^{\Gamma}_{\alpha\beta}(r) \, dA = f^{\Gamma}_{\alpha\beta}(r) \, dN^{\Gamma} \Big/ \int_{r_a}^{r_b} dr r^2 f^{\Gamma}_{\alpha\beta}(r) \tag{A7}$$

and the integration over all the centre distances gives the desired site–site distribution functions $g^{\Gamma}_{\alpha\beta}(r)$. The sum over the configurations Γ produces the total atom–atom distribution functions shown in figure 4(a) and (b). The electronic overlap effects are taken into account by neglecting the contributions to $g^{\Gamma}_{\alpha\beta}(r)$ due to sites whose distance $r_{\alpha\beta}$ is lower than the atomic hard cores which are 3.1, 2.0 and 2.7 Å for N_2, F_2 and Cl_2, respectively. Such values nearly correspond to the r positions at which the experimental or MD $g_{aa}(r)$ start to be different from zero.

References

[1] Rodger P M, Stone A J and Tildesley D J 1988 *Mol. Phys.* **63** 173
[2] Rodger P M, Stone A J and Tildesley D J 1988 *Chem. Phys. Lett.* **145** 365
[3] Bellissent-Funel M C, Buontempo U, Petrillo C and Ricci F P 1990 *Mol. Phys.* **71** 253
[4] Andreani C, Bellissent-Funel M C, Buontempo U, Petrillo C and Ricci M A 1991 *Phys. Rev.* A **44** 5018
[5] Andreani C, Cilloco F and Osae K 1986 *Mol. Phys.* **57** 931
[6] Singer K, Taylor A and Singer J V L 1977 *Mol. Phys.* **33** 1757
[7] Gamba Z and Halac E B 1987 *J. Chem. Phys.* **87** 7184
[8] Stillinger F H and Weber T A 1988 *J. Chem. Phys.* **88** 5123
[9] Misawa M 1989 *J. Chem. Phys.* **91** 2575
[10] De Santis A, Gregori A and Rocca D 1991 *Chem. Phys. Lett.* **181** 579; 1992 *Mol. Phys.* **75** 653; 1993 *Mol. Phys.* **79** 645
[11] De Santis A, Gregori A and Rocca D 1993 *Chem. Phys. Lett.* **213** 239
[12] De Santis A, Gregori A and Rocca D 1994 *Chem. Phys. Lett.* **224** 283
[13] De Santis A, Gregori A and Rocca D 1994 *Mol. Phys.* at press
[14] Andreani C, Dore J C and Ricci F P 1991 *Rep. Prog. Phys.* **54** 683
[15] Hansen J P and McDonald I R 1986 *Theory of Simple Liquids* (London: Academic)
[16] Murthy C S, Singer K, Klein M L and McDonald I R 1980 *Mol. Phys.* **41** 1387
[17] Gray C G and Gubbins K E 1984 *Theory of Molecular Fluids* vol **1** (Oxford: Clarendon) ch 5, p 400, ch 2, p 84
[18] Egelstaff P A, Page D I and Powles J G 1971 *Mol. Phys.* **20** 881
[19] Gradshteyn I S and Ryzhik I M 1980 *Table of Integrals, Series and Products* (New York: Academic)